


Charging at a distance

Troy Shinbrot,* Brandon Jones, and Pranav Saba

Department of Biomedical Engineering, Rutgers University, Piscataway, New Jersey 08816, USA (Received 4 August 2018; revised manuscript received 5 October 2018; published 20 November 2018)

It has been proposed [L. S. McCarty and G. M. Whitesides, *Angew. Chem., Int. Ed.* **47**, 2188 (2008); Lee *et al.*, *Phys. Rev. Mater.* **2**, 035602 (2018)] that contact charging between insulators may be mediated by nonequilibrium transport of adsorbed ions. We remark here that if adsorbed ions transport charges between surfaces, they could equally transport charges across a single surface. We test this hypothesis by contacting initially neutral insulating spheres. We find that localized charge patterns appear very far (centimeters) from a point of contact. We visualize the charges, evaluate their spatial distributions, and discuss mechanisms and implications of this apparent action at a distance.

DOI: [10.1103/PhysRevMaterials.2.115603](https://doi.org/10.1103/PhysRevMaterials.2.115603)

Research over the past decade has revealed that simple contact between insulators produces electrical effects that are anything but simple. For example, experiments in multiple laboratories [1–3] confirm that identical insulators, brought into symmetric contact, charge one another, and oppose the simplest Coulombic considerations by actually *increasing* their charge following repeated contact. Several researchers have also reported nontrivial electrostatic patterning [1,3–6], and most recently it has been demonstrated that between near-contacting surfaces, trapped water reduces its dielectric constant by nearly two orders of magnitude [7].

Theories proposed to explain some of these effects involve mechanisms ranging from nonequilibrium transport of dissociated water ions [8,9] and mechanical production of radicals on contacting surfaces [3,10] to nonlinear amplification of surface dipoles [11,12]. In this paper, we reason that any mechanism that allows charge to flow from one surface to another may also allow charge to flow across a single surface. We experimentally explore this possibility and find in multiple experiments that contact between common insulators produces surface charging *centimeters* away from the contact point.

We begin by visualizing surface charges in the contact electrification experiment depicted in Figs. 1(a) and 1(b). In Fig. 1(a), we sketch contact charging between two common spherical insulators, both attached to insulating posts as shown. The lower insulator is a solid “bouncy ball,” made of polybutadiene, and the upper insulator is a hollow ping-pong ball, made of celluloid. We focus on charging of the hollow ball because the best experimental evidence indicates that contact electrification is predominantly a surface, rather than a bulk, effect [8,13].

Each orange ball shown is drilled through the center with a Forstner bit, which cuts the ball cleanly, and is attached to its post with a nylon screw. A larger hole on one end, visible in Fig. 1(c), is used to accommodate the screw head. The top post is attached to a mechanical shaker that brings the balls into repeated contact. We collide the balls at 10 Hz for 30 s.

The white ball is pierced by a steel blade that is mounted on the post.

Before each trial, the upper ball is washed with alcohol, which in prior experiments was found to effectively discharge it. We have additionally discharged the balls with an active static eliminator (ExAir static ion air gun), but we find that this does not affect the results. After attaching and washing the ball, no contacts are made or broken except at the intended contact point.

Trials have been performed using untreated, hand-sanded, and sand-blasted balls as well: We find that sanding increases the likelihood of producing charge patterns shown in Fig. 1, and in all figures following we identify the preparation of the balls. After colliding the balls, we expose the upper ball to a cloud of bipolar toner to visualize charge patterns. Bipolar toner [1] consists of a mixture of two colors of $\sim 10\text{-}\mu\text{m}$ toner powders, one that charges positively (magenta in Fig. 1) and a second that charges negatively (black) after contact with metal. As sketched in Fig. 1(b), a metal funnel charges the toner, which is entrained in a compressed airflow to produce a cloud of powder.

When a neutral ping-pong ball is exposed to this cloud, little or no powder adheres: Fig. 1(c) shows two sides of a ball neutralized with a static eliminator and then exposed to bipolar toner. When similar balls have been contacted with a bouncy ball, however, charged patterns are readily visible, as shown in Figs. 1(d)–1(f). We note from Fig. 1(d) that the contact points themselves are either neutral or positively charged (black), and are typically surrounded by a charged region of variable sign. On the opposite side of the ball, additional charge patterns are visible. We reiterate that nothing touched the ball after it was cleaned other than at the contact point, and that without contact the ball is expected to exhibit no significant charge patterns [Fig. 1(c)]. We remark that energy is required to separate charges in this way, and this energy comes from mechanical input as described for example in Ref. [14].

Thus it appears that on the side of the ball making contact, charges are transported a small distance to produce patterns near the contact point, and this transport even extends to the other side of the ball, several centimeters away (the

*shinbrot@rutgers.edu

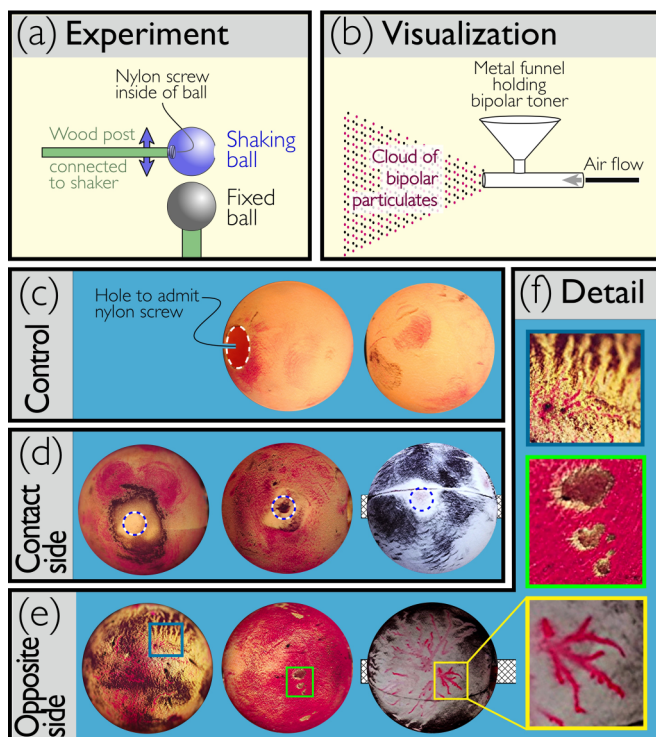


FIG. 1. Contact charge visualizations. (a) Sketch of experiment in which a shaking ball repeatedly contacts a fixed ball. The balls are initially discharged (see text), and the top ball is then brought into contact at 10 Hz for 30 s via an external shaker. Note that by detaching the supporting wood post from the shaker, the top ball can be removed for examination without further contact. (b) Visualization is achieved by blowing bipolar toner (see text) on the balls. (c) Exposure to bipolar toner produces little sticking before shaking. (d) The shaken ball shows a nearly charge-free halo around the contact point (dashed circles), surrounded by charged regions. The orange balls are Mapol 3-star brand, hand sanded with 150- and then 320-grit sandpaper, and the white ball is Kevenz 3-star brand and is unsanded. The orange balls are mounted as depicted in (a); the white ball is pierced with a steel blade (crosshatched), that is connected to the wood post. (e) Remarkably, the *opposite* side of each ball, which was never contacted with anything after initial discharge, shows charge patterns [details of some of these in panel (f)]. Balls are cleaned with alcohol prior to each trial, and all snapshots are deblurred with an unsharp mask.

ping-pong balls are regulation, 4-cm diameter). Charge patterns are highly variable from trial to trial, and include branches, spots, and other features. Patterns appear on both contact and noncontact sides of the upper ball for relative humidities (RH) <40%. At higher humidities, toner still sticks to contacted balls, but patterns become nondescript.

Less variable than patterning details are quantitative measurements of dipole moment, which persist at least to RH \sim 60%. To produce these, we attach two balls (as before, a bouncy ball and a ping-pong ball) to insulating posts. To establish whether distant charging patterns could possibly be associated with either the stress of cutting holes in the balls or interactions with the nylon screw used in Fig. 1, in the experiments measuring dipole moment, the ping-pong balls are intact and are attached to posts using glue. We clean and

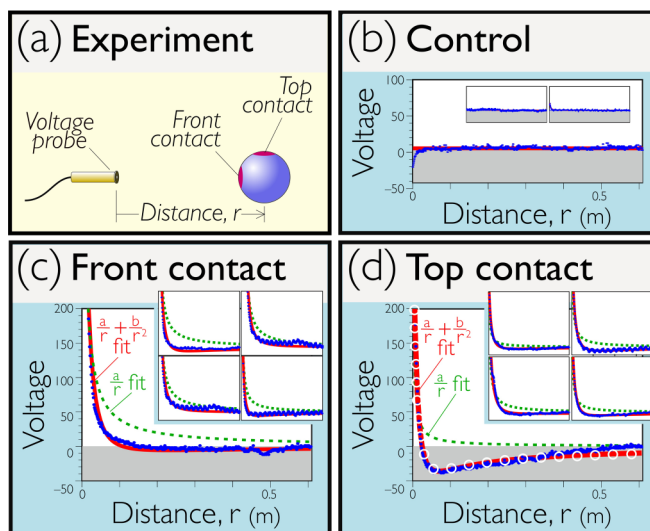


FIG. 2. Discriminating net and dipole charge components. (a) Sketch of experiment, showing charged ball that is pulled a distance r from a noncontact voltage probe. Data are collected for either a ball contacted at a point toward the probe (front contact) or perpendicular (top contact). (b) Control data (blue online) for a discharged ball. (c) Front contact data, including fits to net charge only (dashed, green online) and net plus dipole charge (solid, red online) models. (d) Top contact data, with fits and insets as in panel (c), plus a comparison cubic fit (white circles) described in text. Insets in all panels show additional trials with axes identical to main plots; balls in all cases are unsanded, and RH is above 40%. Balls are discharged with static eliminator (see text) prior to each trial.

discharge the balls and then contact them by simply holding the insulating posts and manually clapping the balls together 20 times. Finally we mount the ping-pong ball on a small carrier together with its attached post, and pull the ball away from a noncontact electrostatic voltmeter probe (Trek model 347).

The idea here is that for a uniformly charged sphere, the voltage will go as $V \sim 1/r$, where r is distance from charge to measurement point, whereas for a dipole the voltage will go as $V \sim 1/r^2$. Since Poisson's equation is linear, we expect superposition to hold, and so we can fit a voltage vs distance plot with $V = C(\frac{q}{r} + \frac{q_d d}{r^2})$, where C is a dimensional constant, to obtain quantitative evaluations of the spatially averaged charge, q , and dipole moment, $q_d d$. In detail, we fit voltage vs distance data with the functions $V_{\text{net}} = V_o + \frac{a}{(r-r_o)}$ and $V_{\text{net+dipole}} = V_o + \frac{a}{(r-r_o)} + \frac{b}{(r-r_o)^2}$, where a , b , and r_o are obtained using nonlinear regression, and V_o is the mean of voltage measurements at the furthest distances. We pull the carrier holding the charged ball through two fixed checkpoints using a string attached to a capstan that is rotated with a dc motor. The checkpoints are spaced 0.61 m apart, which we use to convert the voltage time series to the distance units shown in Fig. 2. Checkpoint crossings are inexact, and we estimate the resulting uncertainty in distance units to be $\pm 10\%$.

Results of this procedure are shown in Figs. 2(b)–2(d) for several cases. In Fig. 2(b), we show control measurements for a discharged ball, confirming both that the ball holds minimal charge and that the measurement process does not add or remove charge, either for the ball or its surroundings.

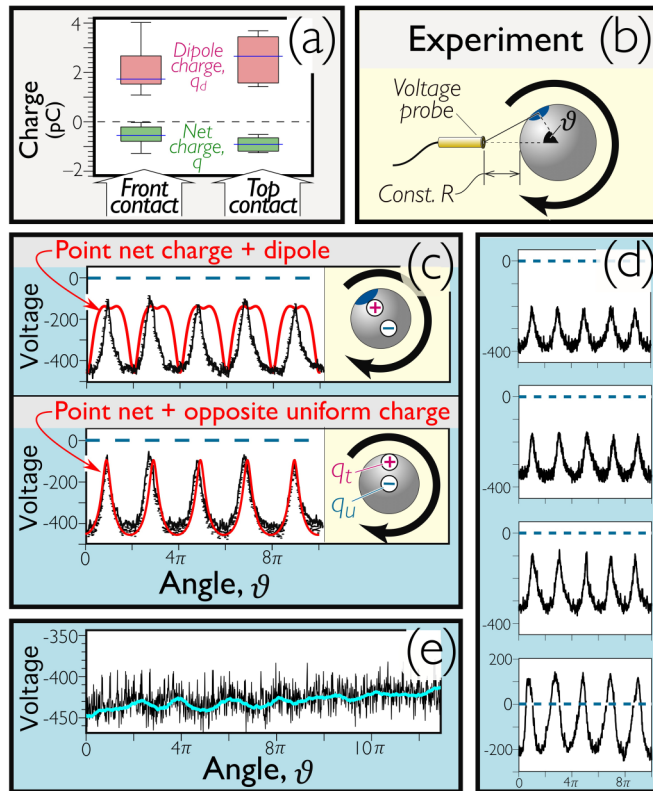


FIG. 3. Quantitative charge distributions. (a) Data collected from fits shown in Figs. 2(c) and 2(d). Coefficients are put into common units by dividing the dipole coefficient by the ball radius (see text). (b) Experiment in which hollow ball is contacted as in Fig. 2, and is then rotated at constant distance from voltage probe. The attached post is perpendicular to the sketch. (c) Voltage vs angle for orange ball contacted 20 times with white ball, fit with trial functions for a point surface charge plus an induced dipole (top), and for a point charge plus a uniform charge (bottom). (d) Replicates of the same experiment, including example at bottom showing positive charge at contact point and negative charge on opposite side of ball. (e) Resulting voltage vs angle data for balls used in Fig. 2; thick line is running average of 1/4 s of data. Orange ball is unsanded Mapol 3-star brand ball, white ball is unsanded Kevenz 3-star brand, and RH is above 40%. Balls are discharged with static eliminator prior to each trial.

In Fig. 2(c), we show the result of the same measurements on a ping-pong ball that has been contacted on its “front”: at a point closest to the probe. In Fig. 2(d), we show the same for a ball contacted on its “top” as identified in Fig. 2(a). Manifestly in all cases, voltage data for contact electrified balls are significantly better fit by the function $V_{\text{net+dipole}}$ than by V_{net} (see Supplemental Material [15] for details). In each of the five trials for front and for top charging, we obtain p values $< 10^{-10}$, and $R^2 > 0.97$ for the individual fits, with standard errors over the five trials $< 10\%$ for both q and q_d .

In Fig. 3(a), we show results collected from all of the experiments of Figs. 2(c) and 2(d). The units of net charge and dipole moment differ, and to present both components in a single plot, we convert a and b to common units of charge by dividing b by the ball diameter, $d = 0.04\text{m}$. Figure 3(a) provides three essential findings.

First, the net and dipole charges are opposite in sign. This is compatible with an induced dipole moment, since induction reduces the voltage near the originating charge.

Second, the net and dipole charges are comparable in magnitude. This is not compatible with an induced dipole, as can be seen by expressing the analytic solution for the potential of a point charge q on the surface of a dielectric sphere of diameter d . This is a standard exercise [16]: for celluloid (the material of ping-pong balls) with dielectric constant $\kappa = 4$, the potential to leading order at distance r and azimuthal angle ϑ is

$$V(r, \vartheta) = \left(\frac{q}{4\pi\epsilon_o} \right) \frac{1}{r} - \left(\frac{q \cdot d}{4\pi\epsilon_o} \right) \frac{1}{2r^2} \cos(\vartheta) + \dots \quad (1)$$

Inserting the ball diameter, $d = 0.04$ m, we obtain

$$V(r, \vartheta) = \left(\frac{q}{4\pi\epsilon_o} \right) \frac{1}{r} - \left(\frac{q}{4\pi\epsilon_o} \right) \frac{1}{100r^2} \cos(\vartheta) + \dots \quad (2)$$

So, a dipole coefficient due to simple induced polarization is expected to be two orders of magnitude smaller than the net charge coefficient, whereas Fig. 3(a) shows that experimentally the dipole coefficient is several times *larger* than the net charge coefficient.

A third finding from Fig. 3(a) is that the dipole coefficient produced by top contact (perpendicular to the probe axis) is comparable to the coefficient produced by front contact (in-line with the probe). This seems counterintuitive, since the cosine term in Eq. (2) implies that top contact should produce vanishing dipole moment.

To understand this counterintuitive finding, we perform a third experiment, in which we manually clap two balls attached to insulating posts 20 times as before, but then rotate one of the balls in front of the voltage probe at constant distance, R , as sketched in Fig. 3(b). Rotating a charged ball in this way produces data shown in Figs. 3(c)–3(e) that we can use to reconstruct the angular distribution of charge. In Fig. 3(c), we contact an orange ping-pong ball 20 times with a white ping-pong ball, as in Fig. 2 but with both balls screwed to insulating rods (as was done in Fig. 1). Replicates of this experiment are shown in Fig. 3(d); shortly we discuss quite different results following collision with a bouncy ball.

The balls are 4 cm in diameter as before and the orange ball is held $R = 1$ cm away from the probe, so a point charge on its surface should produce a voltage: $V \propto 1/\sqrt{5 + 4\cos(\omega t + \delta)}$, where ω is the rotation frequency, t is time, and δ is a phase defining the initial angle of the ball. The fit shown at the top of Fig. 3(c) as a bold curve includes an induced dipole moment with illustrative polarizability $\alpha = 0.12$ (point- and induced charges are sketched to the right of the data). With or without polarizability, this fit has a sharp cusp at the maximum of $|V|$, produced at the closest approach of the point charge.

Evidently, a point surface charge on a dielectric sphere fails to describe the data. On the other hand, a point charge plus a uniform surface charge generates a qualitatively better fit: this is shown in the bottom plot in Fig. 3(c). As indicated in the sketch to the right, the fit here uses a positive point charge on a ball with uniform negative charge. Similarly to Fig. 3(a), the magnitudes of the two charges are comparable (the uniform charge here is 3.6 times the point charge).

For collisions between two ping-pong balls, shown in Figs. 3(c) and 3(d), both perpendicular and in-line dipole moments can be explained by the observation that the voltmeter probe is aligned with the center of the ping-pong ball as shown in Figs. 2(a) and 3(b), and consequently the dipole shown at the bottom right of Fig. 3(c) is vertically offset from the probe axis. The voltage in this geometry is easily derived and obeys $V(r) = \frac{q_u}{r} + \frac{q_t}{\sqrt{r^2 + d^2/4}}$, where q_u and q_t are the uniform and top charges indicated at the bottom-right of Fig. 3(c). Expressed as a power series in $1/r$, this becomes

$$V(r, \pi/2) = \left(\frac{q_u + q_t}{4\pi\epsilon_o} \right) \frac{1}{r} - \left(\frac{q_t \cdot d^2}{4\pi\epsilon_o} \right) \frac{1}{8r^3} + \dots \quad (3)$$

The values of q_u and q_t can be chosen to fit this cubic function to the data of Fig. 2(d), yielding results nearly indistinguishable from the fit of the quadratic function of Eq. (2): The main plot of Fig. 2(d) includes the cubic fit (as white circles) superimposed over the quadratic fit (as a solid curve). Based on this agreement, it is apparent that dipole moments both perpendicular and parallel to the measurement axis can be obtained by the presence of a simple asymmetry in charge distribution.

In the case of collisions with the bouncy ball used in Fig. 2, however, the same orange ball produces data shown in Fig. 3(e), exhibiting inconclusive dependence on rotation angle. The net charges of the two cases shown in Figs. 3(c) and 3(e) are comparable (about -450 V), but the positive point charge that produces the cusps in collisions between ping-pong balls is nearly absent in collisions between a ping-pong ball and a bouncy ball.

From these results we conclude that while asymmetric charges could produce the dipole fits seen in Fig. 2, closer analysis indicates that this asymmetry is not observed, and additional effects must be at work. We cannot account for the difference in rotational data between contact between two ping-pong balls and one of these balls and a bouncy ball, but it seems plausible that differences in mechanical stress [6] and work function [17] affect localized charge distributions. In particular, recent work has demonstrated that contact charging depends on deformation of polymer surfaces [6], which may play an important—and yet to be fully elucidated—role in the charging reported here.

In conclusion, multiple replicates of three experiments indicate that contact between material surfaces can generate charging at a distance, typically taking the form of a contact point charged with one sign (positive for our materials), accompanied by surrounding charges of opposite sign (negative). At low RH, the surrounding charges are typically

patterned and highly variable in detail. At higher RH, fine-scale patterning is not seen, but charging distant from a contact point persists. This distant charging is seen in both cut and intact balls, and in all cases can to a good approximation be described by a superposition of net charge and dipole moment, where the dipole charge is 3 or 4 times stronger than the net charge in common units.

Each of these experiments is reproducible, but at the same time the experiments provide results that defy simple explanations. At low RH, distant charge patterns such as those shown in Fig. 1 invariably appear on both sides of a contacting ball. The patterns differ in detail from trial to trial and include branches and spots, reported previously in triboelectrification experiments [1]. We cannot definitively attribute the patterns seen here either to triboelectrification or to other effects, including Paschen breakdown and mechanical stress, which other work has demonstrated can strongly influence contact charging [6].

At higher RH, evidence of distant charging persists. Far from a charged hollow sphere, the distant charging is consistent with a dominant dipole approximation, but closer to the sphere, more complicated charge distributions appear to be involved. Figure 3 suggests that for some materials, these distributions may be associated with an offset in the center of a dipole from the measurement axis, but for the materials used in Fig. 2, more complicated behaviors seem again to be involved.

All of our experiments agree in demonstrating that regions near a contact point acquire one charge, while more distant regions acquire the opposite. In this respect, perhaps the most perplexing aspect of the experiments is that insulating surfaces somehow perform the magic of liberating enough charge carriers to produce this charge separation, but not enough to discharge it. The charges involved apparently can move distances of centimeters during contact, but cannot move back to neutralize charge gradients over shorter distances. So, it appears likely that multiple charge-transport mechanisms operating over different time- and distance scales are involved in contact charging: a constraint on future models for charging at a distance.

We thank Behrooz Ferdowsi, Matthew VanDusen-Gross, Jeremy Stein, and Sankaran Sundaresan for their help and advice. This work was supported by NSF-DMR, Award No. 1404792.

T.S. conceived and planned the work and wrote the paper, B.J. and P.S. designed and built the apparatus and executed the experiments.

The authors declare no competing interests.

-
- [1] T. Shinbrot, T. S. Komatsu, and Q. Zhao, Spontaneous tribocharging of similar materials, *Europhys. Lett.* **83**, 24004 (2008).
- [2] J. F. Kok and D. J. Lacks, Electrification of granular systems of identical insulators, *Phys. Rev. E* **79**, 051304 (2009).
- [3] H. T. Baytekin, A. Z. Patashinski, M. Branicki, B. Baytekin, S. Soh, and B. A. Grzybowski, The mosaic of surface charge in contact electrification, *Science* **333**, 308 (2011).
- [4] T. Shinbrot, Granular electrostatics: Progress and outstanding questions, *Eur. Phys. J.: Spec. Top.* **223**, 2241 (2014).
- [5] I. S. Aranson, D. Blair, V. A. Kalatsky, G. W. Crabtree, W.-K. Kwok, V. M. Vinokur, and U. Welp, Electrostatically Driven Granular Media: Phase Transitions and Coarsening, *Phys. Rev. Lett.* **84**, 3306 (2000).

- [6] A. E. Wang, P. S. Gil, M. Holonga, Z. Yavuz, H. T. Baytekin, R. M. Sankaran, and D. J. Lacks, Dependence of triboelectric charging behavior on material microstructure, *Phys. Rev. Mater.* **1**, 035605 (2017).
- [7] L. Fumagalli, A. Esfandiar, R. Fabregas, S. Hu, P. Ares, A. Janardanan, Q. Yang, B. Radha, T. Taniguchi, K. Watanabe, G. Gomila, K. S. Novoselov, and A. K. Geim, Anomalously low dielectric constant of confined water, *Science* **360**, 1339 (2018).
- [8] L. S. McCarty, and G. M. Whitesides, Electrostatic charging due to separation of ions at interfaces: Contact electrification of ionic electrets, *Angew. Chem., Int. Ed.* **47**, 2188 (2008).
- [9] V. Lee, N. M. James, S. R. Waitukaitis, and H. M. Jaeger, Collisional charging of individual submillimeter particles: Using ultrasonic levitation to initiate and track charge transfer, *Phys. Rev. Mater.* **2**, 035602 (2018).
- [10] B. H. Baytekin, T. Baytekin, and B. A. Grzybowski. What really drives chemical reactions on contact charged surfaces? *J. Am. Chem. Soc.* **134**, 7223 (2012).
- [11] T. Siu, J. Cotton, G. Mattson, and T. Shinbrot, Self-sustaining charging of identical colliding particles, *Phys. Rev. E* **89**, 052208 (2014).
- [12] R. Yoshimatsu, N. A. M. Araújo, G. Wurm, H. J. Herrmann, and T. Shinbrot, Self-charging of identical grains in the absence of an external field, *Sci. Rep.* **7**, 39996 (2017).
- [13] K. E. Daniels, C. Bauer, and T. Shinbrot, Correlations between electrical and mechanical signals during granular stick-slip events, *Granular Matter* **16**, 217 (2014).
- [14] R. Yoshimatsu, N. A. Araújo, T. Shinbrot, and H. J. Herrmann, Segregation of charged particles under shear, *Granular Matter* **20**, 35 (2018).
- [15] See Supplemental Material at <http://link.aps.org/supplemental/10.1103/PhysRevMaterials.2.115603> for fit parameters for data shown in Fig. 2.
- [16] J. D Jackson, *Classical Electrodynamics* (John Wiley and Sons, New York, 2007), problem 4.9.
- [17] J. C. Larentie, P. Traoré, and L. Dascalescu, Discrete element modeling of triboelectric charging of insulating materials in vibrated granular beds, *J. Electrostat.* **71**, 951 (2013).